

Inertia onset in disordered porous media flow

Damian Śniezek,* Sahrish B. Naqvi,† and Maciej Matyka‡

Institute of Theoretical Physics, University of Wrocław, pl. M. Borna 9, 50-204 Wrocław, Poland

(Dated: March 27, 2024)

We investigate the very onset of the inertial regime in pore-scale fluid flow in a three-dimensional, disordered porous media. We analyze how the flow structure changes with increasing Reynolds number. In particular, we compute tortuosity, spatial kinetic energy localization, and the pore-space volume fraction containing negative streamwise velocity. Our analysis shows that the onset of inertia observed in a standard way by computing the friction factor appears at a Reynolds number two orders of magnitude higher than indicated by analyzing tortuosity and spatial distribution of kinetic energy.

I. INTRODUCTION

One of the most striking phenomena in transport through porous media is the formation of flow channels, determined not only by geometry but by the transport phenomenon itself [1]. Several factors influence fluid behavior in porous media, such as pore size distribution, porosity, permeability, and the complexity of the fluid's pathways, often referred to as tortuosity [2]. Its understanding is fundamental in hydrology, petroleum engineering, environmental science, and chemical engineering. Applications of porous media span across various fields, including microfluidic devices [3], energy production and development [4], and the design of filters [5] and chemical reactors [6], just to name a few. Usually, there are two empirical laws used to describe fluid dynamics in porous media. In creeping, laminar regime, [7, 8] Darcy's law $\mathbf{u} = -\frac{\mathcal{K}}{\mu L}\nabla p$ is used, where \mathbf{u} is the velocity vector, μ the dynamic viscosity of the fluid, \mathcal{K} the permeability of the domain, L the characteristic length of sample, and p the pressure. However, the deviation from linear Darcy's law emerges for higher velocities. There, the nonlinear relationship between the pressure drop and the filtration velocity is described by introducing the Forchheimer term, which is the second order correction to Darcy law: $\mathbf{u} = -\frac{\mathcal{K}}{\mu L}\nabla p - \beta\mathcal{K}|\mathbf{u}|\mathbf{u}$, [9–12], where β is a model parameter scaling the quadratic velocity term. The impact of large-scale permeability heterogeneity on high-velocity flows in porous media was analyzed in [13]. There, an effective inertial coefficient, which was determined from numerical simulations, varied with Reynolds number, variance, and mean permeability ratio differently across serial-layered, parallel-layered, and correlated media.

The boundaries between Darcy and inertial flow regimes in two-dimensional porous media were experimentally observed for the first time in the rod porous medium model [14]. It was shown that the transition between linear and nonlinear regimes occurs for

$1 < Re < 10$. In two-dimensional, disordered porous media, $Re = 0.37$ was indicated [15]. A study utilizing network modeling to analyze the onset of non-Darcy flow in porous media highlighted the significant influence of pore geometry on the critical Reynolds number and the onset of inertial flow [16]. The influence of high fluid velocities on fluid flow and tracer transport in heterogeneous porous media was investigated in [17]. Structural complexity in the media was shown to intensify inertial effects and lead to a more homogenized flow [18]. In consequence, predictable chemical transport patterns were observed.

Our aim is to take an insight into the physical mechanisms that govern the transition of the pore-scale flow to a nonlinear regime. In this work, we study the flow through disordered porous media. We perform fully converged numerical simulations of Navier-Stokes equations in pore scale. In particular, we analyze flow structure, tortuosity, and spatial distribution of kinetic energy at the very onset of the inertial regime.

II. MODEL AND METHOD

Our porous media samples consist of spherical non-overlapping obstacles with a diameter of $D = 1$ randomly distributed in a system with porosity $\varphi = 0.9$ of size $L = (x \times y \times z) = (16D \times 16D \times 16D)$. The sample was placed in the $(66D \times 16D \times 16D)$ empty channel at $x = 20D$ in order to minimize effect of inlet and outlet boundary conditions on the pore-scale flow. We generated eight independent random samples. The steady, laminar, incompressible Navier-Stokes equations govern the flow in pore-space:

$$\nabla \cdot \mathbf{u} = 0 \quad (1)$$

$$\rho(\vec{u} \cdot \nabla)\vec{u} = -\nabla p + \mu\nabla^2\vec{u}, \quad (2)$$

where ρ is the density of fluid, μ is kinematic viscosity of the fluid, $\vec{u} = (u_1, u_2, u_3)$ is the pore-scale velocity field, and p is the pressure. We set a constant, uniform velocity u_{in} at the inlet and a zero pressure gradient at the outlet. All other boundaries, including the obstacles,

* damian.sniezek@uwr.edu.pl

† sahrishbatool.naqvi@uwr.edu.pl

‡ maciej.matyka@uwr.edu.pl

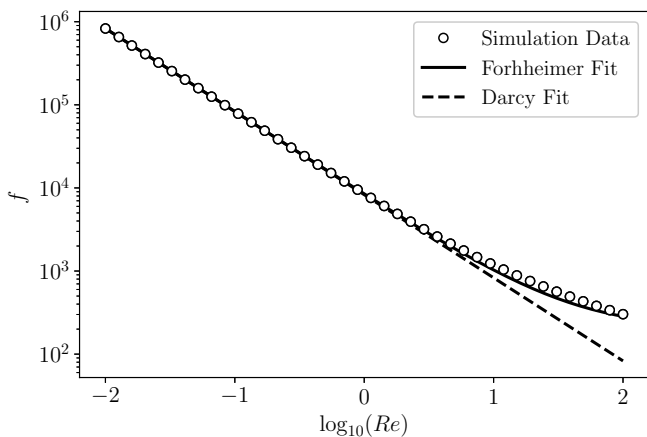


Figure 1. Generalized friction factor f in relation to the Reynolds number. The solid and dashed lines represent the best fit to the Forchheimer and Darcy equations, respectively. The error bars are smaller than the Simulation Data symbols.

are treated as impenetrable solids with no-slip boundary condition. We varied inlet velocity u_{in} , to cover the range of Reynolds numbers $0.01 \leq Re \leq 100$, where $Re = \rho u_{in} D / \mu$. We solved Eqs. (1) and (2) in pore-space using a standard finite volume method. For this we employed a finite volume-based semi-implicit method for pressure-linked equations (SIMPLE algorithm) within the OpenFOAM framework [19]. Our criterion for determining steady-state convergence in the simulations was set to $\epsilon \leq 10^{-6}$, where ϵ was the normalized difference between velocity magnitudes in successive iterations. All simulations were executed in parallel mode using 8-core processors within the OpenMPI library. Domain discretization was accomplished using the standard meshing tools blockMesh and snappyHexMesh of OpenFOAM. To ensure numerical reproducibility, we adopted the standard Richardson extrapolation technique [20, 21].

III. RESULTS AND DISCUSSIONS

First, we identify the flow deviation between Darcy and the inertial regime by calculating the friction factor ($f \equiv -\Delta p / D \beta \rho u^2$) [15] for various Reynolds numbers, shown in Fig. 1. The results are presented as averages from eight independent samples along with the standard error of the mean. This result shows the regime where Darcy's law correctly describes the system. Here, the transition regime appears between $1 \leq Re \leq 10$.

Next, we compute tortuosity to quantify the elongation of fluid pathways [22–25] and their change due to the appearance of inertia. We use the method presented in [2], where it is defined as:

$$\tau = \frac{\langle |\vec{u}| \rangle}{\langle u_1 \rangle}, \quad (3)$$

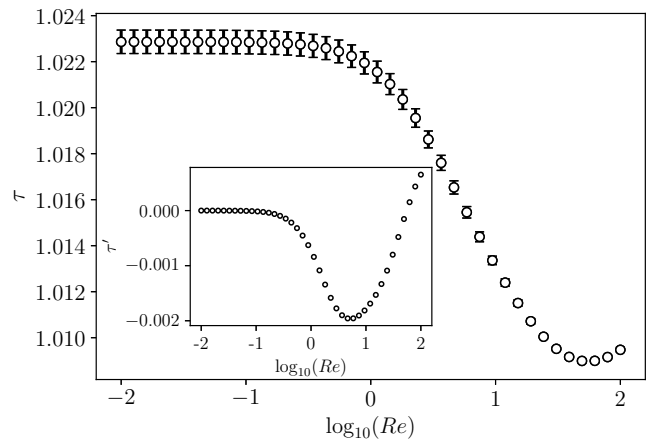


Figure 2. Tortuosity (τ) and its derivative ($\tau' = d\tau/d\log_{10} Re$) (inset).

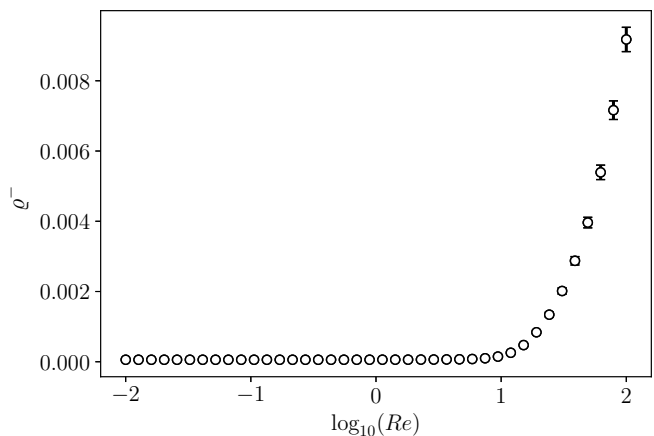


Figure 3. Volume fraction of the pore space with negative streamwise velocity.

where $\langle |\vec{u}| \rangle$ represents the average magnitude of the fluid velocity and $\langle u_1 \rangle$ represents the average streamwise velocity component u_1 in the direction of the flow across the porous sample. In Fig. 2, we plot tortuosity τ versus Re . Tortuosity remains constant in the Darcy regime. It starts decreasing approximately at $Re = 1$, which agrees with [26]. Initially, when the viscous forces are dominating, flow closely follows the pore structure (tortuosity is constant). However, as Re increases and the flow becomes more inertial, the shortening of path lines is visible as tortuosity decreases. The value of τ keeps decreasing till it reaches the minimum value at $Re \approx 62$. After this point, a slight increase is observed, possibly due to the appearance of vortices. Moreover, the decrease of the standard error with increasing Re is noticeable. This suggests a weaker influence of geometry details on the flow structure in higher Reynolds numbers regime. We further show the derivative τ' (inset in Fig. 2) to identify the Reynolds number at which tortuosity starts changing (Fig. 2), which is at $Re \approx 0.1$.

To understand the physical mechanism of tortuosity

decrease at the onset of the inertial regime, we compute the volume fraction of the pore space with negative streamwise velocity u_1 as:

$$\begin{aligned} \varrho^- &= \frac{1}{V_{\text{fluid}}} \int_{V_{\text{fluid}}} f(u_1(\vec{r})) d^3r \\ &\approx \frac{1}{V_{\text{fluid}}} \sum_i^n f(u_1^i) V_i, \end{aligned} \quad (4)$$

where i denotes mesh's cell index, n is the total number of cells, V_i is the i -th cell volume. The function f is defined as:

$$f(u_1) = \begin{cases} 1, & u_1 < 0 \\ 0, & \text{otherwise} . \end{cases} \quad (5)$$

The results of ϱ^- are illustrated in Fig. 3. Interestingly, the Reynolds number at which the backward flow emerges ($Re \approx 10$) is not compliant with Reynolds at which inertia appears, indicated in Fig. 1 and Fig. 2. To understand this, we calculate the spatial distribution of kinetic energy within the porous samples, a statistical measure of the channeling effect [15]. To quantify this phenomenon, we compute the energy localization defined as participation number π [15]:

$$\pi = \left(n \sum_{i=1}^n q_i^2 \right)^{-1}, \quad (6)$$

where $q_i = e_i / \sum_j^n e_j$ is the fraction of the total pore

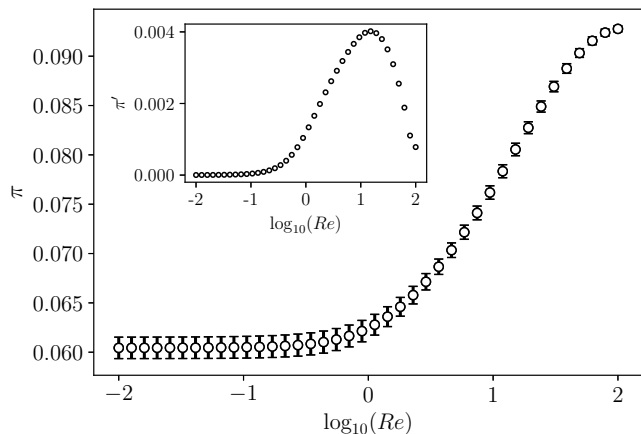


Figure 4. Participation number (π) and its derivative ($\pi' = d\pi/d\log_{10}Re$) (inset).

space kinetic energy contained in the i -th mesh cell. Results of energy distribution are given in Fig. 4. The plot shows a rise of π with the Reynolds number. High value of π indicates a more homogeneous energy distribution, which represents the weakening of the channeling effect. This effect is clearly visible when one compares the streamlines in low and high Re regimes (see Fig. 5). The strong channeling effect at a low Reynolds number

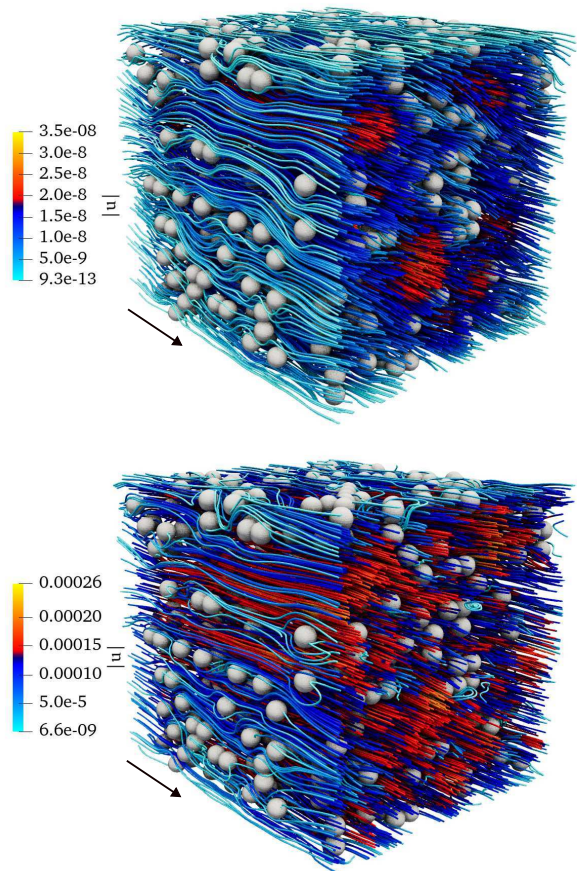


Figure 5. Flow streamlines (colored by velocity magnitude or color intensity in gray-scale) for two Reynolds numbers: $Re = 0.01$ (top) and $Re = 100$ (bottom). The obstacles are shown in white color. The arrows indicate the flow direction.

($Re = 0.01$) is indicated by the fact that only small part of pore space volume give a significant contribution to the transport. With increasing Re , as the kinetic energy is more dispersed in pore space, weakening of the channeling effect is observed. This is visible as the change in colour of streamlines (decreased intensity in grayscale) in Fig. 5. A more dispersed flow channels are clearly visible at higher Reynolds number ($Re = 100$). This shift from preferential channeling to more dispersed flow patterns as Re increases is due to the inertial forces surpassing viscous forces. It causes the fluid flow to spread out and fill more of the available pore space [15]. This agrees with our previous observation in π increase (see Fig. 4). We also observe the presence of backward flow at $Re = 100$, indicated by elongated, highly tortuous streamlines in low-velocity regions which agrees with our results of negative velocity appearance at increasing Re given in Fig. 3. Here, fluid particles are transported along paths that diverge from the previously geometry guided channels. The occurrence of backward flow, and thus vortices, suggests complex flow interactions and is a precursor to turbulent effects that may appear if the Reynolds number increases

further.

IV. CONCLUSIONS

In that study, we investigated what physical phenomena drive the transition from Darcy to the inertial regime in the flow through disordered porous media. Based on the results, we conclude that the physical inertial effects in the flow appear earlier than deviations from the Darcy law. Analysis of tortuosity τ and spatial energy distribution π show visible impact of inertial forces on the flow for $Re \approx 1$. Moreover, derivatives of τ' and π' are non-zero already at $Re \approx 0.1$. The weakening of the channeling effect with increasing Re is also visible for $Re > 1$ in streamline visualization. On the other hand, vortices appear at $Re \approx 10$ as indicated by the emergence of the backward flow in pore space. At approximately the same Re , the maximum of π' is observed. This indicates that vortices in pore space limit the kinetic energy dispersion

in the system by excluding part of the pore space volume available for the main transport.

ACKNOWLEDGEMENT

Funded by National Science Centre, Poland under the OPUS call in the Weave programme 2021/43/I/ST3/00228. This research was funded in whole or in part by National Science Centre (2021/43/I/ST3/00228). For the purpose of Open Access, the author has applied a CC-BY public copyright licence to any Author Accepted Manuscript (AAM) version arising from this submission.

The authors are thankful for Dawid Strzelczyk's support, his in-depth discussions, and insights into this work. We are also grateful to Josè S. Andrade Jr. for insightful discussion and comments during the early stages of the work.

-
- [1] J. D. Hyman, Flow channeling in fracture networks: characterizing the effect of density on preferential flow path formation, *Water Resources Research* **56**, e2020WR027986 (2020).
- [2] M. Matyka, A. Khalili, and Z. Koza, Tortuosity-porosity relation in porous media flow, *Physical Review E* **78**, 026306 (2008).
- [3] S. C. Cao, J. Jung, and M. Radonjic, Application of microfluidic pore models for flow, transport, and reaction in geological porous media: From a single test bed to multifunction real-time analysis tool, *Microsystem technologies* **25**, 4035 (2019).
- [4] A. Banerjee and D. Paul, Developments and applications of porous medium combustion: A recent review, *Energy* **221**, 119868 (2021).
- [5] Y. Zhang, Y. Zhou, Y. Zhang, Z. Zhang, J. Liu, J. Zhu, Z. Sun, L. Li, and H. Gu, Optimal design of silver-loaded zeolite filter structure based on porous media model, *Separation and Purification Technology* **334**, 125905 (2024).
- [6] F. Wang, Y. Shuai, Z. Wang, Y. Leng, and H. Tan, Thermal and chemical reaction performance analyses of steam methane reforming in porous media solar thermochemical reactor, *International Journal of Hydrogen Energy* **39**, 718 (2014).
- [7] S. P. Neuman, Theoretical derivation of darcy's law, *Acta mechanica* **25**, 153 (1977).
- [8] S. Whitaker, Flow in porous media i: A theoretical derivation of darcy's law, *Transport in porous media* **1**, 3 (1986).
- [9] P. Basak, Non-darcy flow and its implications to seepage problems, *Journal of the irrigation and drainage division* **103**, 459 (1977).
- [10] S. Whitaker, The forchheimer equation: a theoretical development, *Transport in Porous media* **25**, 27 (1996).
- [11] Z. Zeng and R. Grigg, A criterion for non-darcy flow in porous media, *Transport in porous media* **63**, 57 (2006).
- [12] S. Arbabi and M. Sahimi, The transition from darcy to nonlinear flow in heterogeneous porous media: I—single-phase flow, *Transport in Porous Media* , 1 (2024).
- [13] M. Fourar, R. Lenormand, M. Karimi-Fard, and R. Horne, Inertia effects in high-rate flow through heterogeneous porous media, *Transport in Porous Media* **60**, 353 (2005).
- [14] A. Dybbs and R. Edwards, A new look at porous media fluid mechanics—darcy to turbulent, *Fundamentals of transport phenomena in porous media* , 199 (1984).
- [15] J. Andrade Jr, U. Costa, M. Almeida, H. Makse, and H. Stanley, Inertial effects on fluid flow through disordered porous media, *Physical Review Letters* **82**, 5249 (1999).
- [16] M. Veyskarami, A. H. Hassani, and M. H. Ghazanfari, A new insight into onset of inertial flow in porous media using network modeling with converging/diverging pores, *Computational Geosciences* **22**, 329 (2018).
- [17] A. Nissan and B. Berkowitz, Inertial effects on flow and transport in heterogeneous porous media, *Physical Review Letters* **120**, 054504 (2018).
- [18] A. Zolotukhin and A. Gayubov, Analysis of nonlinear effects in fluid flows through porous media, *Journal of Petroleum Exploration and Production Technology* **12**, 2237 (2022).
- [19] H. Jasak, A. Jemcov, Z. Tukovic, *et al.*, Openfoam: A c++ library for complex physics simulations, in *International workshop on coupled methods in numerical dynamics*, Vol. 1000 (2007) pp. 1–20.
- [20] P. J. Roache *et al.*, Quantification of uncertainty in computational fluid dynamics, *Annual review of fluid Mechanics* **29**, 123 (1997).
- [21] J. Cadafalch, C. Pe' rez Segarra, R. Consul, and A. Oliva, Verification of finite volume computations on steady-state fluid flow and heat transfer, *J. Fluids Eng.* **124**, 11 (2002).
- [22] L. Green Jr and P. Duwez, Fluid flow through porous metals, *Journal of Applied Mechanics* **18**, 39 (1951).

- [23] F. Thauvin and K. Mohanty, Network modeling of non-darcy flow through porous media, *Transport in Porous Media* **31**, 19 (1998).
- [24] J. Cooper, X. Wang, and K. Mohanty, Non-darcy-flow studies in anisotropic porous media, *SPE Journal* **4**, 334 (1999).
- [25] M. Coles and K. Hartman, Non-darcy measurements in dry core and the effect of immobile liquid, in *SPE Gas Technology Symposium* (OnePetro, 1998).
- [26] R. Sivanesapillai, H. Steeb, and A. Hartmaier, Transition of effective hydraulic properties from low to high reynolds number flow in porous media, *Geophysical Research Letters* **41**, 4920 (2014).
- [27] H. Stanley, A. Araujo, U. Costa, and J. Andrade Jr, Fluid flow through disordered porous media, *Fractals* **11**, 301 (2003).
- [28] S. Rojas and J. Koplik, Nonlinear flow in porous media, *Physical Review E* **58**, 4776 (1998).
- [29] M. G. Gerritsen and L. J. Durlofsky, Modeling fluid flow in oil reservoirs, *Annu. Rev. Fluid Mech.* **37**, 211 (2005).
- [30] J. Fohring, E. Haber, and L. Ruthotto, Geophysical imaging of fluid flow in porous media, *SIAM Journal on Scientific Computing* **36**, S218 (2014).
- [31] K. Wu, M. I. Van Dijke, G. D. Couples, Z. Jiang, J. Ma, K. S. Sorbie, J. Crawford, I. Young, and X. Zhang, 3d stochastic modelling of heterogeneous porous media—applications to reservoir rocks, *Transport in porous media* **65**, 443 (2006).
- [32] M. Ezzatabadipour and H. Zahedi, A novel method for streamline-based tortuosity calculation and investigation of obstacles shape effect on tortuosity in porous media with random elliptical obstacles using lattice boltzmann method, *Transport in Porous Media* **136**, 103 (2021).